Band-structure calculations, and magnetic and transport properties of ferromagnetic chromium tellurides (CrTe, Cr_3Te_4, Cr_2Te_3)

J. Phys.: Condens. Matter **1** (1989) 9141–9161. Printed in the UK

Band-structure calculations, and magnetic and transport properties of ferromagnetic chromium tellurides (CrTe, Cr_3Te_4, Cr_2Te_3)

J Dijkstra†§, H H Weitering†, C F van Bruggen†, C Haas† and R A de Groot‡

† Laboratory of Inorganic Chemistry, Materials Science Centre of the University, Nijenborgh 16, 9747 AG Groningen, The Netherlands

‡ Research Institute for Materials, Faculty of Science, Toernooiveld, 6525 ED Nijmegen, The Netherlands

Received 1 March 1989

Abstract. Electronic band-structure calculations are presented for the ferromagnetic compounds CrTe, Cr_3Te_4 and Cr_2Te_3. In these compounds the Cr 3d–Te 5p covalency and the Cr $3d_{z^2}$–Cr $3d_{z^2}$ overlap along the *c* axis are the most important interactions. The magnetic polarisation of Te is parallel to the Cr local moment in CrTe, antiparallel to it in Cr_2Te_3 and about zero in Cr_3Te_4. Measurements of electronic transport properties (resistivity, Hall effect and thermo-electric power) and magnetic properties of $Cr_{1-\delta}Te$ ($\delta = 0.1$) and $Cr_{3-x}Te_4$ ($x = 0.2$) indicate that these chromium tellurides are p-type metals, with strong interaction between the holes in the Te 5p band and the Cr magnetic moments. In the literature the variation of the magnetic properties of $Cr_{3.2}Te_4$ near $T_s \simeq 100$ K has been attributed to a change from a canted antiferromagnetic to a collinear ferromagnetic structure. However, our Hall-effect measurements indicate that the spin structure is not collinear ferromagnetic above T_s.

1. Introduction

Compounds of chromium tellurides have attracted much attention since the discovery of ferromagnetism in 'CrTe' (Haraldsen and Neuber 1935). In the system $Cr_{1-x}Te$ ($0 < x < 0.375$) various phases have been discovered. The chromium tellurides are ferromagnetic, with Curie temperatures T_C between 180 and 340 K, and have metallic conductivity. Ipser *et al* (1983) determined the phase diagram of Cr–Te and found the following phases: (i) hexagonal $Cr_{1-x}Te$, with a minimum value of x of 0.1; (ii) monoclinic Cr_3Te_4; (iii) trigonal Cr_2Te_3; and (iv) trigonal and monoclinic Cr_5Te_8.

In this paper we will concentrate on the first three compounds: $Cr_{1-x}Te$, Cr_3Te_4 and Cr_2Te_3. Results of band-structure calculations of CrTe, Cr_3Te_4 and Cr_2Te_3 in the collinear ferromagnetic spin arrangement are reported in § 3. In §§ 4 and 5 measurements of transport and magnetic properties on $Cr_{1-x}Te$ and Cr_3Te_4 are presented. Measurements of the anomalous Hall effect are reported in § 6.

The crystal structures of the chromium tellurides have in common a (distorted) hexagonal close packing of Te atoms, with Cr atoms in octahedral interstices, while Cr vacancies occur in every second metal layer. The vacancy ordering within the layers can

§ Present address: Philips Research Laboratories, PO Box 80000, 5600 JA Eindhoven, The Netherlands.

0953-8984/89/469141 + 21 $02.50

be influenced by thermal treatment (Hashimoto and Yamaguchi 1969) and may induce small deviations from hexagonal symmetry (Chevreton *et al* 1963, Chevreton 1964). A comparison of the results reported by different authors is hampered by the inaccurate determination of stoichiometry and vacancy ordering and by the structural instability of quenched alloys (Grazhdankina *et al* 1976b).

Hexagonal $Cr_{1-x}Te$ is a ferromagnet with a Curie temperature T_C of ~340 K, a saturation moment at 4.2 K of about 2.4–2.7 μ_B and an effective paramagnetic moment μ_{eff} of ~4.0 μ_B (Lotgering and Gorter 1957, Hirone and Chiba 1960, Ohsawa *et al* 1972). The value of the saturation moment cannot be understood from an ionic description ($Cr^{2+}Te^{2-}$: Cr $3d^4 \rightarrow 4\mu_B$). This difference is not due to orbital contributions, which are small, since the measured g-factor is 2.01 (Grazhdankina and Zaynullina 1971).

Under the influence of high pressure the Curie temperature is reduced and at 28 kbar and 100 K the ferromagnetism disappears, as can be concluded from electron spin resonance (Shanditsev *et al* 1973) and neutron diffraction (Lambert-Andron *et al* 1979).

According to Ipser *et al* (1983) the Cr_3Te_4 phase has a rather large existence range, from 53.5 to 59 at.% Te. The best criterion to distinguish the Cr_3Te_4 phase from the $Cr_{1-x}Te$ phase is the slight monoclinic lattice distortion in Cr_3Te_4, which accompanies the vacancy ordering within the metal layers. According to this criterion, the compounds Cr_5Te_6 and Cr_7Te_8 reported earlier in the literature belong to the $Cr_{1-x}Te$ or Cr_3Te_4 phase. The Curie temperatures observed for Cr_3Te_4 phases are 315–340 K, dependent on the exact Cr concentration. The paramagnetic effective moment is about 4.2 μ_B, while the saturation magnetisation at 4.2 K is 2.35 μ_B per Cr (Bertaut *et al* 1964, Hashimoto and Yamaguchi 1969, Yamaguchi and Hashimoto 1972). The lower value of the saturation moment is caused by the presence of a canted ferromagnetic structure at low temperatures, clearly observed with neutron diffraction (Andresen 1963, 1970, Bertaut *et al* 1964, Starichenko 1978, Makovetskii and Shakhlevich 1979). At a transition temperature T_s of 80–115 K, dependent on stoichiometry (Yamaguchi and Hashimoto 1972), the antiferromagnetic reflections in the neutron diffractogram disappear, which is usually interpreted as a transition to a collinear ferromagnetic state. While the above-mentioned neutron diffraction studies agree on the occurrence of a canted antiferromagnetic state, they propose different spin structures and various values (between 2 μ_B and 4 μ_B) for the local magnetic moments on Cr.

Cr_3Te_4 phases show metallic conductivity and, like $Cr_{1-x}Te$, a strong decrease of T_C with pressure. The transition temperature T_s increases strongly with increasing pressure (Grazhdankina *et al* 1976a).

The third compound to be discussed is Cr_2Te_3. The crystal structure, with Cr vacancies ordered in every second metal layer, is described in § 2. Cr_2Te_3 is ferromagnetic with T_C = 170–180 K and μ_{sat}(4.2 K) = 2.0 μ_B per Cr. From susceptibility measurements one deduces $S = 1.545$ ($\mu_{eff} = 3.96\ \mu_B$) per Cr, close to the spin-only value of Cr^{3+} (Andresen 1963, 1970, Hashimoto *et al* 1971). The magnetic moments of Cr in the fully occupied layers are ferromagnetically aligned and have an average value of 2.6 μ_B, while the Cr atoms in the partially filled layers give only a small contribution to the neutron diffractograms; they possibly have a spiral spin arrangement or they have no magnetic moment at all (Andersen 1970, Hamasaki *et al* 1975).

2. Crystal structures

The basic structure of $Cr_{1-x}Te$ is the hexagonal NiAs structure, space group $P6_3/mmc$ or D^4_{6h} (No 194 in the *International Tables of Crystallography*), with the Cr atoms at the

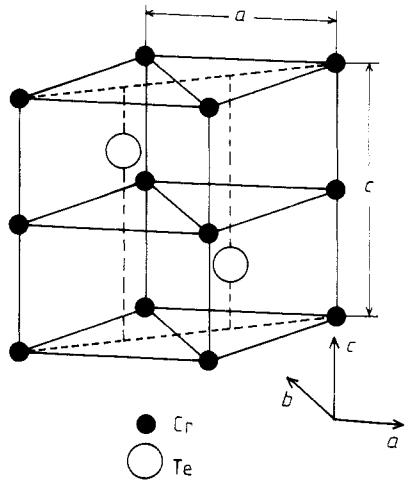

Figure 1. The NiAs-type crystal structure of CrTe.

(2*a*) sites (0, 0, 0) and (0, 0, $\frac{1}{2}$) and Te atoms at the (2*c*) sites ($\frac{1}{3}$, $\frac{2}{3}$, $\frac{1}{4}$) and ($\frac{2}{3}$, $\frac{1}{3}$, $\frac{3}{4}$). The hexagonal unit cell is shown in figure 1. The cell parameters are $a_0 = 3.997$ Å and $c_0 = 6.222$ Å at room temperature (Chevreton *et al* 1963). The Cr–Te distance is 2.78 Å. The c_0/a_0 ratio of 1.557 is smaller than the ideal value of 1.633. Six Te atoms form a trigonally distorted octahedron around Cr. A Cr atom is further surrounded by six other Cr atoms in the *ab* plane at a distance of $a_0 = 3.997$ Å, but much shorter metal–metal distances are present along the *c* axis: a Cr atom has two Cr neighbours at $c_0/2 = 3.111$ Å.

In the non-stoichiometric phase $Cr_{1-x}Te$ there is a (partial) ordering of the Cr vacancies in alternate metal layers, resulting in the trigonal space group $P\bar{3}m1$ or D^3_{3d}.

The unit cell of stoichiometric monoclinic Cr_3Te_4 can be described in the space group I_2/m or C^3_{2h} (No 12 in the *International Tables of Crystallography*), (Bertaut *et al* 1964) with the atoms at the special positions:

	(0, 0, 0), ($\frac{1}{2}$, $\frac{1}{2}$, $\frac{1}{2}$) +
2 Cr_1 in (2*c*)	(0, 0, 0)
4 Cr_2 in (4*i*)	$\pm(x, 0, z)$ with $x = 0.022$ and $z = 0.240$
4 Te_1 in (4*i*)	$\pm(x, 0, z)$ with $x = 0.336$ and $z = 0.866$
4 Te_2 in (4*i*)	$\pm(x, 0, z)$ with $x = 0.329$ and $z = 0.879$.

The unit cell is four times as large as that of $Cr_{1-x}Te$, doubled in the *c* direction and in the *ab* plane ($a \simeq \sqrt{3}a_0$, $b \simeq a_0$, $c \simeq 2c_0$ and the angle between $\boldsymbol{a}$ and $\boldsymbol{b}$ is now 90°, where a_0 and c_0 are the lattice parameters of the corresponding CrTe (NiAs-type) unit cell). The lattice parameters *a*, *c*, a_0 and c_0 at room temperature are given in table 1. The positions of the Cr atoms are shown in figure 2. The Cr vacancies occur in every second metal layer and they are also ordered in the vacancy layers itself. The Cr_1 atoms, i.e. the Cr atoms in the vacancy layers, are coordinated by two Cr_2 atoms along the *c* direction, at a short distance 0.24*c*. The Cr_2 atoms, situated in the fully occupied metal layers, have along the *c* axis only one Cr_1 neighbour. On the other side is a Cr vacancy.

In our band-structure calculation the angle β between the *ab* plane and the *c* axis is approximated to be 90° instead of the real value $\beta = 91.17°$, so that an orthorhombic unit cell results.

Table 1. Crystal-structure parameters (Å) and Wigner–Seitz sphere radii (Å) used in the band-structure calculations.

	CrTe[a]	Cr_3Te_4[b]	Cr_2Te_3[c]
a axis	3.997	3.934	6.823
c axis	6.222	12.34	11.80
b axis	—	6.879	—
a_0 axis	3.997	3.934	3.933
c_0 axis	6.222	6.170	5.900
c_0/a_0	1.557	1.568	1.500
$V(Cr_xTe)$ (Å^3)	43.05	41.35	39.52
r_{Cr}	1.223	1.240	1.313
r_{Te}	2.037	2.005	1.931
$r_{emptysphere}$	—	1.240	1.313

[a] Chevreton *et al* (1963).
[b] Chevreton (1964).
[c] Hamasaki *et al* (1975).

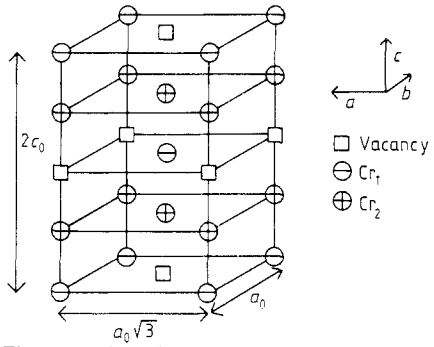

Figure 2. Chromium atoms and vacancies in the crystal structure of Cr_3Te_4.

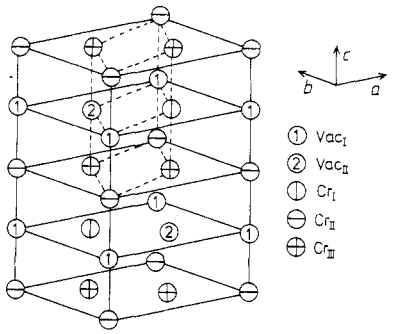

Figure 3. Chromium atoms and vacancies in the crystal structure of Cr_2Te_3.

The crystal structure of Cr_2Te_3, shown in figure 3, can be described in the space group $P\bar{3}1c$ or D^2_{3d} (No 163 in the *International Tables of Crystallography*), with the atoms on the special positions (Bertaut *et al* 1964, Hamasaki *et al* 1975):

2 Cr_I in (2*c*) $\pm(\frac{1}{3}, \frac{2}{3}, \frac{1}{4})$

2 Cr_{II} in (2*b*) $(0, 0, 0)$ and $(0, 0, \frac{1}{2})$

4 Cr_{III} in (4*f*) $\pm(\frac{1}{3}, \frac{2}{3}, z)$, $\pm(\frac{1}{3}, \frac{2}{3}, \frac{1}{2} - z)$ with $z \simeq 0$

12 Te in (12*i*) (x, y, z) etc. with $x = 0.320$, $y = -0.004$ and $z = 0.374$.

Here *a* and *c* are doubled compared with the NiAs-type unit cell. The Cr vacancies lie in every second metal layer. In the vacancy layer one-third of the positions are occupied by Cr_I atoms, which have two Cr_{III} neighbours on $c_0/2 = 2.95$ Å. The Cr_I atoms have no direct Cr neighbours in the *ab* plane. The Cr_{II} and Cr_{III} atoms together form the fully

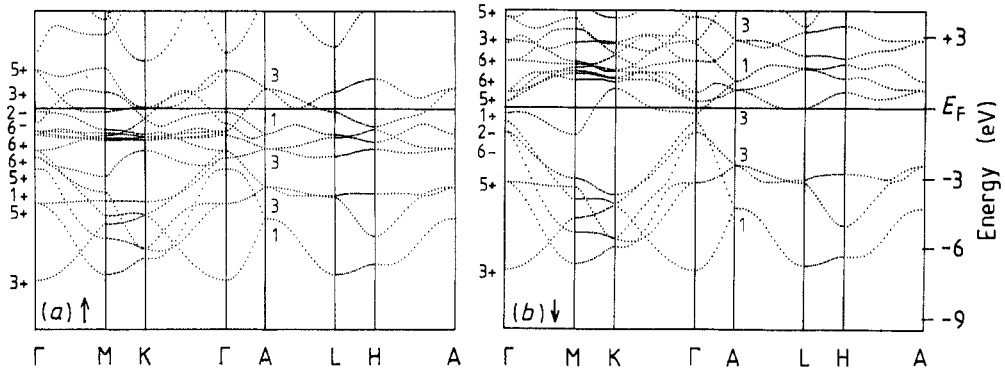

Figure 4. The energy bands along the high-symmetry directions of the Brillouin zone of ferromagnetic CrTe for majority (*a*) and minority (*b*) spin.

occupied metal layers. Cr_{II} has no Cr neighbours along the *c* axis and Cr_{III} has only one Cr_I neighbour along the *c* axis.

3. Band-structure calculations

Electronic band-structure calculations of CrTe, Cr_3Te_4 and Cr_2Te_3 are performed for a collinear ferromagnetic arrangement of the Cr magnetic moments. The band structure of CrTe is also calculated with a collinear antiferromagnetic spin arrangement and in the non-magnetic state.

The band-structure calculations were performed using the augmented spherical wave (ASW) method of Williams *et al* (1979). Exchange and correlation were treated in the local density approximation (Hedin and Lundquist 1971). Scalar relativistic effects were included as described by Methfessel and Kübler (1982). Spin–orbit effects were neglected. Inclusion of spin–orbit interaction in the band-structure calculation of the compound MnSb, where the spin–orbit interaction is comparable in magnitude, results in splittings of states of no more than a few tenths of an electronvolt and only small details in the band structure are altered (Coehoorn *et al* 1985).

In the ASW method the crystal is divided into so-called Wigner–Seitz spheres around each atom. The sum of the volumes of these spheres is equal to the unit cell volume. Empty spheres are included on the vacancy sites of Cr_3Te_4 and Cr_2Te_3. Within the Wigner–Seitz spheres the potential is taken to be spherically symmetric. Partial densities of states are obtained by calculating the eigenvalues on a regular mesh of points in the irreducible part of the Brillouin zone. The calculations are self-consistent. The input and output charges within each Wigner–Seitz sphere differed less than 10^{-5} electron in the last iteration. The basis functions were composed of 4s, 4p and 3d functions on Cr; 5s, 5p and 5d functions on Te; and 1s and 2p functions on the empty spheres. Cr 4f and Te 4f functions were included in the internal summation of the three-centre contributions to the matrix elements.

3.1. CrTe

The crystal parameters and Wigner–Seitz sphere radii used in the band-structure calculations of CrTe are given in table 1. The calculated energy bands along high-symmetry

directions in the hexagonal Brillouin zone of ferromagnetic CrTe (F–CrTe) for both spin directions are shown in figure 4. The majority, spin-up direction is indicated by ↑ and the minority, spin-down direction by ↓. In Γ and A the symmetry notation of Miller and Love (1967) is used. In the ALH plane all bands are twofold degenerate. In figure 5 the total and partial densities of states (DOS) are plotted. In figure 6 the Te DOS is decomposed into contributions of the different angular momentum quantum numbers l. The band at 12.5 eV binding energy is of Te 5s origin. From an ionic point of view one should say that the next six bands 3–8, counting from the bottom of figure 4, are the Te 5p bands and that the following 10 bands (9–18) are Cr 3d bands. However, strong hybridisation between the Cr 3d and the Te 5p states is observed, while also Te 5d states are mixed in (figures 5 and 6). For convenience, however, we will still speak about these bands as Cr 3d, etc.

The Cr 3d bands show an exchange splitting between ↑ and ↓ spin of 2.87 eV, while they are 4.7 and 5.0 eV wide, respectively. The different number of occupied majority and minority states gives a magnetic moment of 3.51 μ_B per formula unit CrTe. The major part of this magnetisation, 3.29 μ_B, is found within the Cr Wigner–Seitz sphere, but

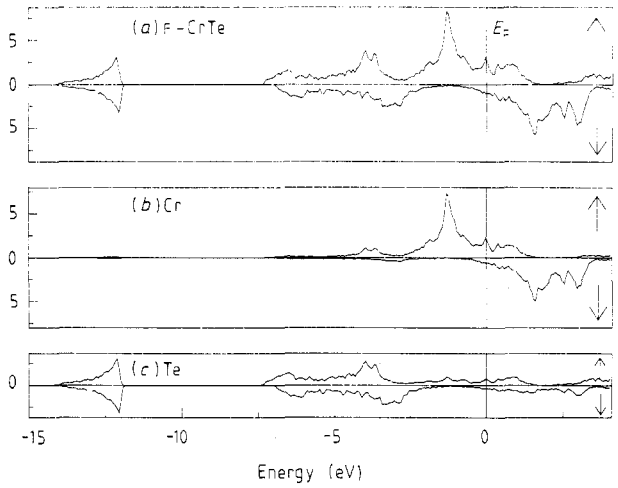

Figure 5. (*a*) Total density of stages (DOS) of ferromagnetic CrTe for majority (↑) and minority (↓) spin. (*b*) Partial Cr DOS. (*c*) Partial Te DOS. Units: states/(eV unit cell).

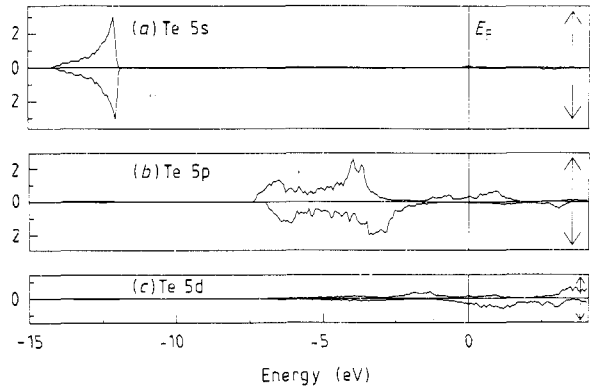

Figure 6. The angular-momentum contributions to the partial Te DOS of F-CrTe.

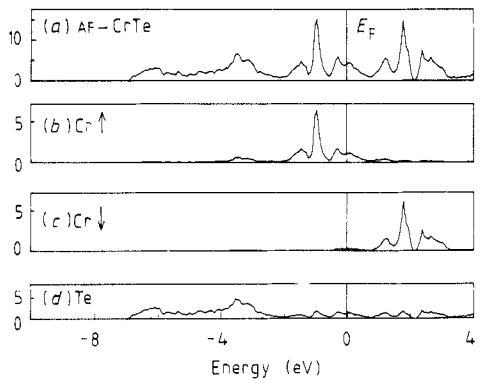

Figure 7. (*a*) Total DOS of antiferromagnetic CrTe. (*b*) Sublattice A: ↑ Cr DOS. (*c*) Sublattice A: ↓ Cr DOS. (*d*) Te DOS. Units: states/(eV unit cell).

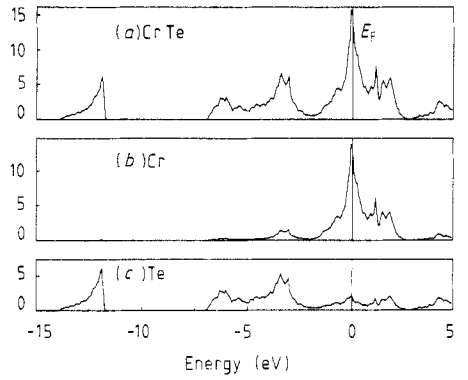

Figure 8. (*a*) Total DOS of non-magnetic CrTe. (*b*) Partial Cr DOS. (*c*) Partial Te DOS. Units: states/(eV unit cell).

through the strong Cr 3d–Te 5p covalency also some magnetisation density ($+0.22\ \mu_B$) is induced on the Te atoms. That the calculated moment is smaller than the $4\ \mu_B$ expected for Cr^{2+} (high-spin d^4) can be understood from the fact that also the Cr 3d ↓ band partly lies below E_F (band 9, in Γ_{1+} and in M). A wavefunction analysis shows this band to be mainly composed of a bonding combination of Cr $3d_{z^2}$ states. These states point along the *c* axis, the direction in which every Cr atom has two Cr neighbours at a rather short distance. The Cr $3d_{z^2}$ states form a band along the *c* direction (ΓA), with extrema at Γ, resulting from bonding (Γ_{1+}) and antibonding (Γ_{3+}) combinations of $3d_{z^2}$ states on neighbouring Cr atoms.

A simple way to understand the calculated band structure starts with an ionic description followed by introduction of hybridisation effects. This can best be illustrated on the basis of the minority-spin band structure. We can concentrate on ΓA in figure 4(*b*). The energy values in A give an indication of the centres of mass of different bands. The dispersion in the $A\Gamma$ direction is caused by interactions along the *c* direction. The lowest eigenvalue in A (A_1) has mainly Te $5p_z$ character and the next state with A_3 symmetry has Te $5p_x$ and $5p_y$ character. Above E_F we find an A_3 and an A_1 state close together, which are the Cr 3d t_{2g} states, and about 1.8 eV higher lies another A_3, the Cr 3d e_g states. The Cr t_{2g}–e_g ligand-field splitting of 1.8 eV is caused by the (trigonally distorted) octahedral coordination of Cr by six Te. The t_{2g} bands are essentially non-bonding, while the e_g bands are shifted to higher energies through interaction with the Te states. From the A_1 (a_{1g}) state of the t_{2g} manifold two dispersive bands appear ending in Γ_{1+} and Γ_{3+}. These are the Cr $3d_{z^2}$ states, which have a large interaction in the *c* direction; the bonding–antibonding splitting amounts to 3.1 eV. The other two bands of the t_{2g} manifold in A mainly have $3d_{xy}$ and $3d_{x^2-y^2}$ character; they hardly have any overlap in the *c* direction and consequently no disperison in the ΓA direction. The Cr e_g states, the highest A_3, are of $3d_{xz}$ and $3d_{yz}$ character and thus show a dispersion along ΓA, which lies in magnitude in between the two cases mentioned before. The Te 5p states show a similar behaviour: the $5p_z$ bands show a much larger dispersion along ΓA ($A_1 \rightarrow \Gamma_{3+}/\Gamma_{2-}$) than the $5p_x$ and $5p_y$ derived bands ($A_3 \rightarrow \Gamma_{5+}/\Gamma_{6-}$).

In the majority-spin band structure in principle the same analysis can be made, but here the situation is obscured by the stronger covalent mixing of states with the same symmetry.

For comparison also the electronic structure of CrTe with an antiferromagnetic (AF) spin arrangement is calculated. The simplest antiferromagnetic structure was used: antiparallel moments on the two Cr sites in the unit cell, i.e. ferromagnetic sheets in the *ab* plane, coupled antiparallel along the *c* axis. This spin structure is observed for other compounds with the NiAs structure, such as CrSb and MnTe (Lotgering and Gorter 1957). In the calculation the two Cr atoms in the unit cell, representing the two magnetic sublattices A and B, were treated independently. Lattice parameters and Wigner–Seitz sphere radii were the same as used for F-CrTe (see table 1).

The total DOS of AF-CrTe is shown in figure 7 together with the spin-up and spin-down DOS for one Cr sublattice, called A, and the Te partial DOS. The second Cr sublattice, B, has an identical partial DOS as A, only the role of $\uparrow$ and $\downarrow$ is interchanged. Within the Cr Wigner–Seitz spheres a magnetic moment of 3.174 μ_B is found. The Te atoms carry no net magnetisation by symmetry. The exchange splitting between the Cr 3d $\uparrow$ and 3d $\downarrow$ peaks in the DOS is 2.77 eV. The density of states at the Fermi level is about the same as for F-CrTe.

In the preceding section it was shown that the large width of the 3d bands in F-CrTe is caused by the Cr 3d–3d interactions, of which the $3d_{z^2}$–$3d_{z^2}$ hybridisation along the *c* axis, the direction of the shortest Cr–Cr distance, is the strongest. In the AF arrangement neighbouring spins along the *c* axis are antiparallel. So the centres of mass of the 3d bands of one spin direction on neighbouring Cr sites along the *c* axis differ by the exchange splitting, ~2.8 eV, while in F-CrTe they lie at the same energy. As a consequence, with equal d_{z^2}–d_{z^2} overlap parameters the broadening of the Cr 3d band due to metal–metal interaction is much smaller in the AF than in the F case. In the following paper the relative stability of the ferromagnetic or the antiferromagnetic spin structure in Cr monochalcogenide compounds is discussed in more detail (Dijkstra *et al* 1989).

Finally a band-structure calculation of non-magnetic CrTe is performed. In the calculated DOS, shown in figure 8, the Cr–Te covalency is evident. Band widths are comparable to those of F-CrTe. A very large DOS at the Fermi level is found, $N(E_F)$ = 15.2 states/(eV unit cell). This makes the non-magnetic state unstable with respect to the ferromagnetic state. The calculated DOS of non-magnetic CrTe is very similar to the DOS of isoelectronic MnAs and MnSb (Motizuki *et al* 1986, Katoh and Motizuki 1987), calculated in the non-magnetic state by the APW method. The total d/p band widths are similar, only the ionicity is somewhat larger in CrTe than in the before-mentioned Mn compounds. This can be seen from the separation between the peak in the Cr/Mn 3d band and the highest-lying peak in the anion p band, which is 3.2 eV in CrTe and about 2.0 eV in MnAs and MnSb.

3.2. Cr_3Te_4

One of the reasons for performing this study of the electronic structure of chromium tellurides was to investigate whether there are any half-metallic ferromagnets among them. A magnetic compound is called half-metallic if it is metallic for one spin direction, while the Fermi level falls in a band gap for the other spin direction, i.e. if the electrons at E_F are completely spin-polarised. This phenomenon was discovered by de Groot *et al* (1983) in the Heusler alloy NiMnSb. Later it was also found in calculations for other Heusler alloys (de Groot *et al* 1986), Fe_3O_4 (Yanase and Siratori 1984) and CrO_2 (Schwartz 1986). We found that F-CrTe is not half-metallic, since one Cr 3d $\downarrow$ band crosses E_F. As shown in § 4.1 this band mainly consists of Cr $3d_{z^2}$ orbitals, which form bonding combinations along the *c* axis. Generally one would expect that introducing Cr

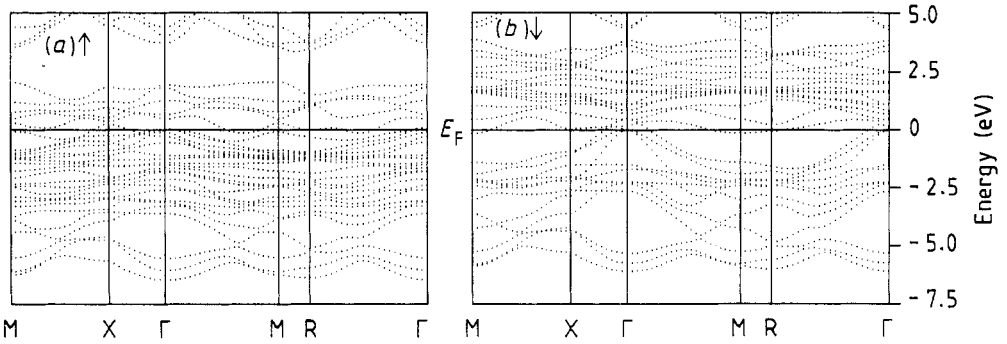

Figure 9. The energy bands along the high-symmetry directions of the Brillouin zone of ferromagnetic Cr_3Te_4 for majority (*a*) and minority (*b*) spin.

vacancies will diminish these metal–metal interactions and reduce the Cr 3d ↓ band width and consequently lift this band above E_F.

The band-structure calculation of Cr_3Te_4 was performed with the orthorhombic unit cell, described in § 3, and a collinear ferromagnetic spin structure, which is assumed to exist between ~100 K and the Curie temperature 340 K (see § 1). The lattice parameters and Wigner–Seitz sphere radii used in the calculation are given in table 1. Figure 9 shows the calculated energy bands along some high-symmetry directions in the Brillouin zone. The DOS of Cr_3Te_4 (figure 10) show much resemblance to the DOS of F-CrTe (figure 5): the Te 5s band at −12 eV below E_F, the Te 5p band between −7 and +3 eV and the exchange-split Cr 3d states, mainly below E_F for ↑ and above E_F for ↓. The Cr_I atoms in the half-filled metal layers have a slightly larger magnetic moment (3.35 μ_B) than the Cr_2 atoms in the completely filled layers (3.29 μ_B). This difference between the magnetic moments of the two types of Cr atoms is much smaller than what one could expect from an ionic picture with Cr_I^{2+} (d^4, 4 μ_B) and Cr_2^{3+} (d^3, 3 μ_B). The trend of higher magnetic moments on the Cr atoms in the vacancy layers is observed by neutron diffraction, where moments of 3.36 and 3.00, respectively, were found (Andresen 1970). Within the Te spheres a small magnetisation is calculated: +0.11 and −0.09 μ_B for Te_1 and Te_2, respectively. The total calculated moment per formula unit is thus 9.96 μ_B.

For a half-metallic compound the magnetic moment per unit cell has to be an integer, since the Fermi level falls in a band gap for one spin direction. This is not the case in F-Cr_3Te_4. An accurate inspection of the energy bands shows that the top of the Te 5p derived band of the minority-spin direction is situated in Γ at 0.5 eV above E_F (see figure 9), while the bottom of the Cr 3d ↓ band lies just (0.2 eV) below E_F. The result is a band overlap between the Cr 3d ↓ and the Te 5p ↓ bands of 0.7 eV. The Cr 3d ↓ band is narrower in Cr_3Te_4 than in F-CrTe, due to the breaking of many Cr–Cr bonds along the *c* axis, but not narrow enough to open a gap in the minority-spin direction. The total DOS at the Fermi level $N(E_F)$ = 6.04, $N^{\uparrow}(E_F)$ = 4.96 and $N^{\downarrow}(E_F)$ = 1.08 states/(eV unit cell).

3.3. Cr_2Te_3

The third compound in the chromium telluride family for which the electronic structure is calculated is Cr_2Te_3. Its crystal structure is given in § 2. Neutron diffraction patterns of this compound could best be fitted by assuming ferromagnetic moments of about 2.6 μ_B on the Cr atoms in the fully occupied layers (Cr_{II} and Cr_{III}), whereas the Cr_I atoms

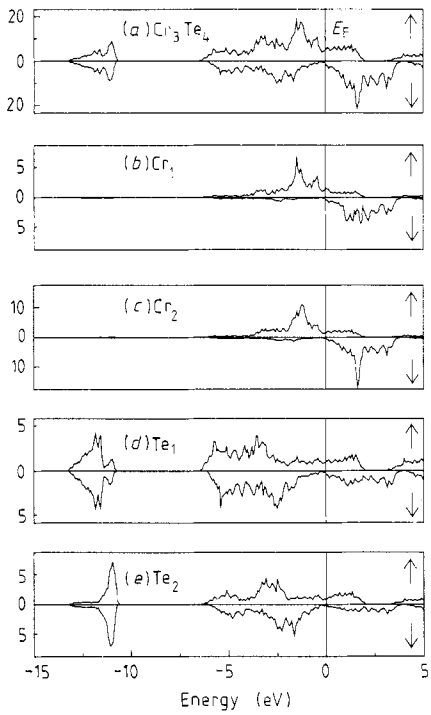

Figure 10. (*a*) Total DOS of ferromagnetic Cr_3Te_4. (*b*) Partial Cr_1 DOS. (*c*) Partial Cr_2 DOS. (*d*) Partial Te_1 DOS. (*e*) Partial Te_2 DOS. Units: states/(eV unit cell).

in the vacancy layers have a negligible ferromagnetic component (Andresen 1970, Hamasaki *et al* 1975).

The lattice parameters and Wigner–Seitz sphere radii used in the calculation are given in table 1. Empty spheres are included on the vacancy sites (2*a*): $\pm(0, 0, \frac{1}{4})$ and (2*d*): $\pm(\frac{2}{3}, \frac{1}{3}, \frac{1}{4})$. The starting potentials were identical for all three kinds of Cr atoms.

Figure 11 shows the energy bands along the high-symmetry directions in the Brillouin zone. In figure 12 the DOS of F-Cr_2Te_3 is shown, together with the partial contributions from the constituent atoms. The Cr partial DOS consists almost completely of 3d states. The Te band at 12 eV below E_F is composed of 5s states and the band between -7 and $+3$ eV of 5p states, with some Te 4d mixed in. Within the Cr Wigner–Seitz spheres magnetic moments of 3.28, 3.29 and 3.32 μ_B, for Cr_I, Cr_{II} and Cr_{III} respectively, are found (Cr_I is situated in the vacancy layer, Cr_{II} and Cr_{III} together form the occupied layer). The Te atoms are antiferromagnetically polarised with $-0.18\,\mu_B$ per Te. The total magnetisation per unit cell (Cr_8Te_{12}) is 24.26 μ_B, equivalent to 3.03 μ_B per Cr. As in F-Cr_3Te_4 this value is non-integer, indicating that Cr_2Te_3 is not a half-metallic ferromagnet. A small DOS at E_F for the minority-spin direction is found; some dispersive Te 5p bands do cross E_F and the top of this band is situated in Γ at 0.65 eV above E_F (see figure 11). At about the same energy a distinct peak is observed in the $\downarrow$ DOS, which consists of Cr 3d states. Wavefunction analysis shows that this peak, which forms the bottom of the Cr 3d $\downarrow$ band, is due to bonding combinations of the Cr $3d_{z^2}$ states along the *c* axis. Its greatest partial contribution comes from Cr_I, which has two Cr neighbours along *c*. Also Cr_{III}, with one Cr neighbour in that direction, contributes, while Cr_{II}, which has vacancies on both sides, has no partial DOS at that energy. All Cr 3d $\downarrow$ bands lie above the Fermi level.

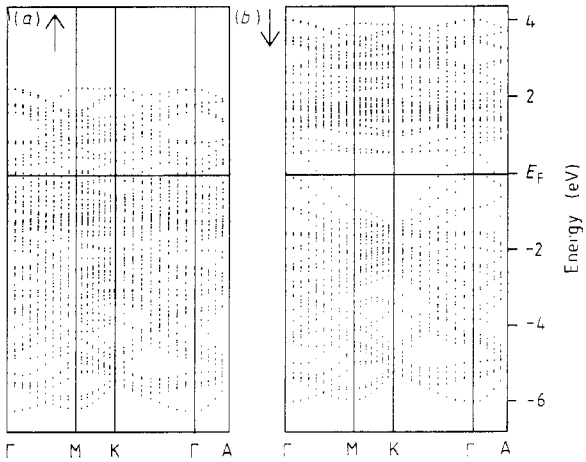

Figure 11. The energy bands along the high-symmetry directions of the Brillouin zone of ferromagnetic Cr_2Te_3 for majority (*a*) and minority (*b*) spin.

3.4. Discussion

We would like to emphasise that it is only a matter of nomenclature to speak of Cr 3d bands, etc., because especially the Cr 3d e_g states and the Te 5p states are strongly mixed. For instance, the top of the Cr 3d $e_g \uparrow$ band at ~1 eV above E_F consists only of 60% of Cr 3d e_g states and 40% of Te 5p states (see figure 5). Further, metal–metal interactions are of importance in these ferromagnetic NiAs (derived) structures with short metal distances along the *c* axis.

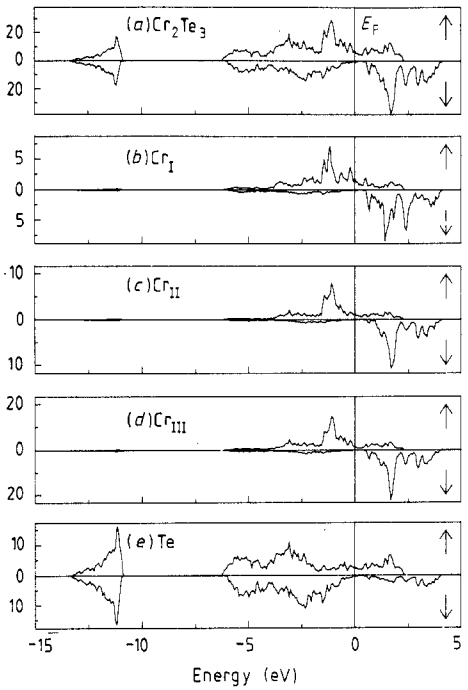

Figure 12. (*a*) Total DOS of ferromagnetic Cr_2Te_3. (*b*) Partial Cr_I DOS. (*c*) Partial Cr_{II} DOS. (*d*) Partial Cr_{III} DOS. (*e*) Partial Te DOS. Units: states/(eV unit cell).

Table 2. Some calculated properties of ferromagnetic Cr–Te compounds. Total magnetisation M per Cr atom and magnetic moments μ within Wigner–Seitz spheres in μ_B; exchange splitting between ↑ and ↓ in eV.

	CrTe	Cr_3Te_4	Cr_2Te_3
M	3.51	3.32	3.03
μ_{Cr}	3.29	3.31	3.30
μ_{Te}	+0.22	+0.01	−0.18
ΔE_{exch}	2.87	2.82	2.74

In order to compare the calculated band structures of CrTe, Cr_2Te_3 and Cr_3Te_4, some parameters are tabulated in table 2. First of all, the calculated total magnetisation per Cr atom decreases with decreasing Cr concentration. In Cr_3Te_4 and Cr_2Te_3 the calculated total magnetisation is close to the value expected in an ionic description with Te^{2-}. In Cr_3Te_4 two Cr^{3+} (d^3) plus one Cr^{2+} (d^4) would give 10 μ_B per Cr_3Te_4, corresponding to an average value of 3.333 μ_B per Cr. The band-structure calculation gives a value of 9.96 μ_B. In Cr_2Te_3 two Cr^{3+} (d^3) would give 6 μ_B per Cr_2Te_3. For CrTe the total moment is less than expected on the basis of an ionic description, cf. 3.51 μ_B instead of the expected 4 μ_B. This is caused by the formation of a band, mainly consisting of bonding combinations of Cr $3d_{z^2}$ states, which partly sinks below E_F for the minority-spin direction. Furthermore metal–metal interactions also shift some antibonding Cr 3d ↑ to higher energies above E_F. In the other two compounds many of these metal–metal bonds are broken due to the presence of vacancies. The bottom of the Cr 3d ↓ band shifts to a higher energy with respect to E_F with increasing number of vacancies. In Cr_2Te_3 all Cr 3d ↓ bands lie above the Fermi level.

The magnetic moments within the Cr Wigner–Seitz spheres are about the same, 3.30 ± 0.02 μ_B, in the three compounds. The variation of the total magnetisation per Cr atom can for a large part be ascribed to the magnetic polarisation of the anions. In CrTe the Te polarisation is parallel to that of the local Cr moments, in Cr_2Te_3 it is antiparallel and in Cr_3Te_4 the mean value of the Te polarisation is about zero. Cr–Te covalency is the origin of the magnetic polarisation of the anions. Generally, a decrease of the number of electrons on a cation—with unchanged valency of the anion—is coupled with a decrease in the electronegativity difference. By changing Cr from '2+' to '3+' the Cr 3d states sink in energy relative to the top of the Te 5p band, which causes the sign change of the Te polarisation as shown in figure 13.

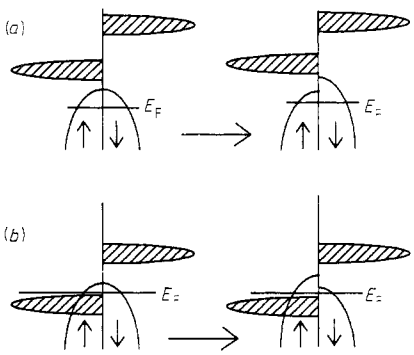

Figure 13. Schematic DOS of chromium tellurides around E_F. The left-hand side and the right-hand side show the Cr 3d and the Te 5p bands without and with covalent mixing, respectively. Dependent on the relative position of the Cr 3d and Te 5p bands, the covalency causes (*a*) a positive or (*b*) a negative magnetic polarisation of the Te 5p band.

From the high-temperature paramagnetic susceptibilities of chromium tellurides values of μ_{eff} are derived: 4.5 μ_B for $Cr_{1-\delta}Te$ (Ohta *et al* 1981), 4.3 μ_B for Cr_3Te_4 (Ohta 1985, Bertaut *et al* 1964) and 3.97 μ_B for Cr_2Te_3. The number of unpaired electrons q_c, calculated via $\mu_{eff} = [q_c(q_c+2)]^{1/2}$, is 3.6, 3.4 and 3.1, respectively, in reasonable agreement with our calculated spin-only values (table 2).

In view of the fact that the paramagnetic susceptibility and the band-structure calculations give moments of 3 μ_B and higher, the low values of the saturation magnetisation at 4.2 K ($\sim$2.4 μ_B, see § 1) must be explained by non-collinear spin structures. Such structures are found by (powder) neutron diffraction, but the complete spin structure was not resolved. The many neutron diffraction studies (Bertaut *et al* 1964, Andresen 1963, 1970, Starichenko 1978, Makovetskii and Shakhlevich 1979, Lambert-Andron *et al* 1979, Hamasaki *et al* 1975) give no decisive answer about the exact spin structure and the magnitude of the Cr local magnetic moment. Most investigators report that the diffractograms of hexagonal $Cr_{1-\delta}Te$ between 0 K and T_C as well as of monoclinic Cr_3Te_4 in the temperature range between T_s (100 K) and T_C can be described in terms of a collinear ferromagnetic structure, but more intricate spin structures cannot be ruled out.

If indeed the spin structure is collinear ferromagnetic, the reduced values of the saturation magnetisation of CrTe should perhaps be explained in terms of the spin fluctuation theory of Moriya (1985). The q_c/q_s ratio—q_c is the number of Bohr magnetons derived from the saturation magnetisation and q_s from the paramagnetic susceptiblity—used in the Rhodes–Wohlfahrt plot (Wohlfahrt 1978) is then 3.6/2.4 = 1.5. This is much larger than the value of 1, expected for local-moment ferromagnets.

A breakdown of the itinerant electron picture, as in NiO (Zaanen *et al* 1985, Zaanen 1986), due to electron–electron interactions is not very likely in CrTe, because of the broad 3d bands and strong Cr–Te covalency. Also the effective d–d Coulomb interaction U_{eff} is rather small for Cr^{2+} (Zaanen *et al* 1985, Zaanen 1986). Since the Te 5p bands cross the Fermi level, the chromium tellurides are p-type metals.

The fact that band-structure calculations give a good description of the properties of MnAs, MnSb and MnBi (Sandratskii *et al* 1981, Coehoorn *et al* 1985, Coehoorn and de Groot 1985, Katoh and Motizuki 1987), which are isoelectronic and isostructural to CrTe, is another indication that CrTe can be described by a band picture, although CrTe will be slightly more ionic than these manganese pnictides.

An accurate neutron diffraction study on well characterised single crystals of $Cr_{1-\delta}Te$, Cr_3Te_4 and Cr_2Te_3 would be desirable to reveal the exact spin structure and the local magnetic moments on Cr.

4. Experimental results of physical properties of $Cr_{1-\delta}Te$ and Cr_3Te_4

In ferromagnetic materials there exists, in addition to the normal Hall effect due to the Lorentz force on the charge carriers, a second contribution to the Hall effect, which is called the anomalous or spontaneous Hall effect (Berger and Bergmann 1980). This anomalous Hall effect arises from the asymmetric scattering of charge carriers in ferromagnetic or ferrimagnetic materials and is commonly described by an extra term in the Hall resistivity, proportional to the total magnetisation. The anomalous Hall effect offers an opportunity to study the magnetic properties of a material by measuring a transport property.

We have measured the Hall effect, the magnetisation, the specific resistivity and the

thermo-electric power of hexagonal $Cr_{1-\delta}Te$ with $\delta = 0.1$ ($Cr_{0.9}Te$) and monoclinic $Cr_{3+x}Te_4$ with $x = 0.2$ ($Cr_{0.8}Te$).

Homogeneous polycrystalline powders were obtained by heating together the elements at 1200 °C for one week, followed by quenching to room temperature, repowdering and annealing for two weeks at 800–1150 °C. In order to achieve the highest possible Cr content, quenching from 1150 °C is necessary (Ipser *et al* 1983). The polycrystalline compound obtained was shown by x-ray diffraction to be trigonal, with the Cr vacancies in alternating metal layers and cell parameters $a = 4.020$ Å and $c = 6.267$ Å. Chemical analysis gave a nominal composition of $Cr_{0.90}Te$.

Single crystals of Cr_3Te_4 were grown by vapour transport in a temperature gradient from 1000 to 850 °C, using iodine as transport gas, followed by slowly cooling to room temperature. Guinier–Hägg diffraction patterns could be indexed on the basis of the monoclinic space group I2/m with $a = 6.911$ Å, $b = 3.947$ Å, $c = 12.408$ Å and $\beta = 90.68°$ at room temperature. This structure was confirmed by measurements made using a four-circle kappa diffractometa CAD4F (Enraf-Nonius), but refinements were not possible due to the fact that the crystals were triplets. However, it was possible to determine the mean occupation of the layers; the fully occupied layers were more than 99% occupied, while the occupation of the vacancy layers was 56%. This corresponds to a composition $Cr_{0.78}Te$, in agreement with the result of $Cr_{0.80}Te$ obtained by chemical analysis.

4.1. Magnetic properties

Magnetisation isotherms of polycrystalline $Cr_{0.9}Te$ were measured between 4.2 and 300 K, using a Faraday balance. The applied field $B_a = \mu_0 H_a$ varied from 0 to 3 T. The field gradient was 1 T m^{-1}. The saturation magnetisation M_S was derived from the measured isotherms by extrapolating the high-field magnetisation to an applied field $B_a = N_D M$, corresponding to an internal field $B_i = \mu_0 H_i = B_a - N_D M = 0$; N_D is the demagnetising factor.

The saturation magnetisation of $Cr_{0.9}Te$ decreases monotonically with increasing temperature (figure 14 (curve A)). No sign of a magnetic phase transition around 100 K is observed. The spontaneous magnetisation at 4.2 K corresponds to a magnetic moment of 2.70 μ_B per Cr atom, in accordance with previous studies (Hashimoto and Yamaguchi

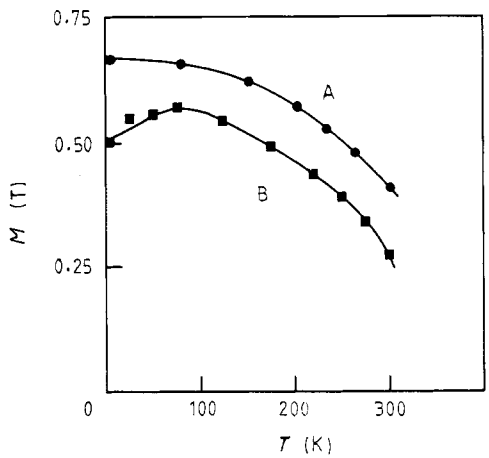

Figure 14. Temperature dependence of the magnetisation of hexagonal $Cr_{0.9}Te$ (curve A) and monoclinic $Cr_{0.8}Te$ (curve B).

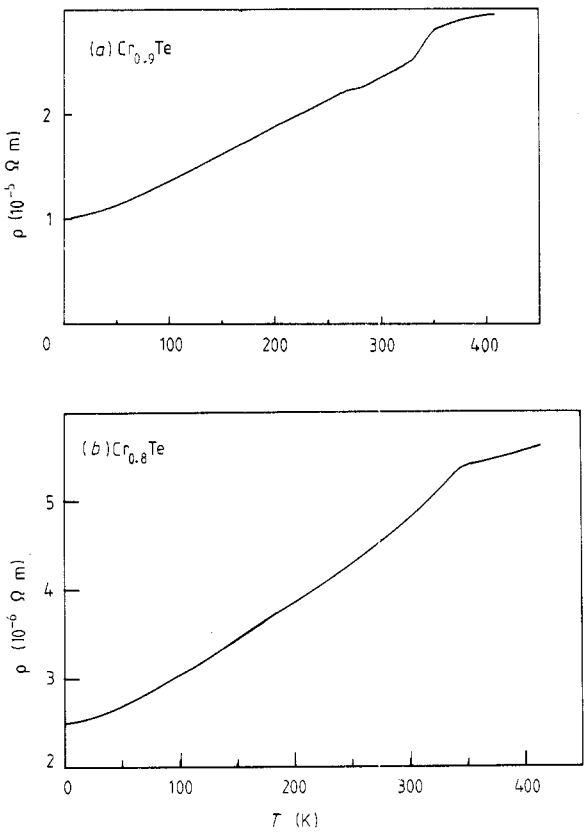

Figure 15. Temperature dependence of the specific resistivity of (*a*) hexagonal $Cr_{0.9}Te$ and (*b*) monoclinic $Cr_{0.8}Te$.

1969, Ohsawa *et al* 1972, Grazhdankina *et al* 1976a, b). This value is considerably lower than the spin-only value of 4 μ_B for d^4.

The saturation magnetisation M_S of single-crystalline monoclinic $Cr_{0.8}Te$ shows a maximum at $T_s \simeq 100$ K (figure 14 (curve B)). Below T_s the magnetisation increases with increasing temperature. It is commonly assumed that at T_s there is a change from a canted ferromagnetic structure at low temperatures to a collinear ferromagnetic structure (see § 1). The magnetisation at 4.2 K corresponds to a magnetic moment of 2.32 μ_B per Cr.

4.2. Electrical resistivity

Both polycrystalline, hexagonal $Cr_{0.9}Te$ and single-crystalline monoclinic $Cr_{0.8}Te$ show metallic conductivity (figure 15). As usual in ferromagnetic metals there are three contributions to the resistivity:

(i) A residual resistivity ρ_{res}, which mainly originates from lattice defects and crystallographic disorder already present at zero temperature. These effects are temperature-independent and consequently ρ_{res} is temperature-independent. For $Cr_{0.9}Te$ a very large residual resistivity $\rho_{res} = 1.0 \times 10^{-5}$ Ω m is observed. For the single-crystalline platelet of $Cr_{0.8}Te$, a lower residual resistivity is found, namely $\rho_{res} = 2.5 \times 10^{-6}$ Ω m.

(ii) A spin-disorder resistivity ρ_{sd}, caused by the scattering of the charge carriers at the magnetic moments. Owing to the disordering of the spins with increasing tem-

perature, ρ_{sd} increases with temperature up to the Curie temperature T_C. Above T_C the spin disorder is maximum. For $Cr_{0.8}Te$, $\rho_{sd} = 1.6 \times 10^{-6}\,\Omega\,m$ at T_C ($\simeq$340 K). For $Cr_{0.9}Te$, this contribution is difficult to determine because the phonon contribution to the resistivity cannot be estimated accurately from the measured resistivity above T_C.

(iii) A phonon contribution, which, for not too low temperatures, is linear with T. The phonon contribution can be determined from the slope of $\partial\rho/\partial T$ above T_C, where the residual and spin-disorder contributions are approximately constant. For $Cr_{0.8}Te$, $\partial\rho/\partial T = 3.5 \times 10^{-9}\,\Omega\,m\,K^{-1}$.

The Curie temperature is clearly discernible in the specific resistivity of both compounds as the temperature where there is a change in the slope of $\partial\rho/\partial T$, which is at 350 K for $Cr_{0.8}Te$ and at 340 K for $Cr_{0.9}Te$. Around $T_s \simeq 100$ K, where a maximum in the magnetisation of $Cr_{0.8}Te$ is observed (figure 14 (curve B)), *no* anomaly is observed in the specific resistivity.

4.3. Thermo-electric power

The thermo-electric power α of both $Cr_{0.8}Te$ and $Cr_{0.9}Te$ was measured between 4.2 and 350 K (figure 16). The two curves show a similar behaviour: an approximately linear temperature dependence, from zero at 4.2 K to $-25\,\mu V\,K^{-1}$ at 350 K. The observed negative sign of α indicates the presence of (relatively heavy) electrons at the Fermi level. A calculation of the Fermi energy from α requires too many approximations to be meaningful. The observed value of α is close to the values reported for other compounds with a not too high, but definitely metallic, conductivity.

No anomaly of the Seebeck coefficient of $Cr_{0.8}Te$ was observed at T_s.

4.4. Normal and anomalous Hall effect

The Hall resistivity ρ_{yx} of ferromagnetic metals can be written as

$$\rho_{yx} = R_0 B + \mu_0 R_S M$$

where R_0 and R_S are the normal and spontaneous or anomalous Hall coefficient, respectively, M is the magnetisation and B is the internal magnetic induction, which is related to the applied magnetic field H_A by $B = \mu_0[H_A + (1 - N_D)M]$, where N_D is the demagnetising factor.

4.4.1. $Cr_{0.9}Te$. The Hall resistivity ρ_{yx} was measured as a function of applied magnetic field (up to 3 T) in the temperature range 4.2–340 K (figure 17), on the same polycrystalline sample of $Cr_{0.9}Te$ that was used for the resistivity measurements. The form

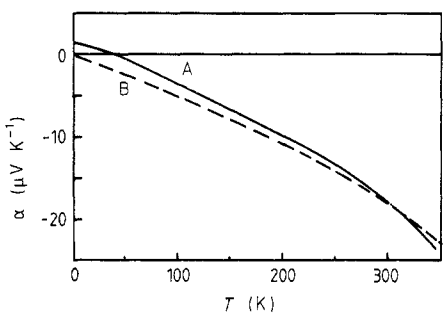

Figure 16. Thermo-electric power α of hexagonal $Cr_{0.9}Te$ (curve A) and monoclinic $Cr_{0.8}Te$ (curve B).

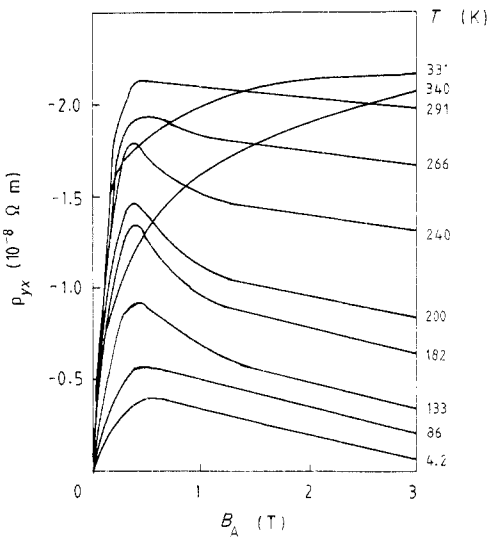

Figure 17. Hall resistivity ρ_{yx} of hexagonal $Cr_{0.9}Te$.

of the ρ_{yx} isotherms is a consequence of the magnetisation process. With increasing field ρ_{yx} increases, because the magnetisation increases, until the applied field reaches the value of the demagnetising field $-N_D M$. At fields of 1 T and higher, the magnetisation is saturated. The spontaneous part of the Hall effect is then constant and the observed variation of ρ_{yx} with field is mainly due to the normal Hall effect. The non-linear behaviour found between 0.5 and 1 T in the temperature range from 130 to 260 K is due to magnetic anisotropy.

The spontaneous contribution to ρ_{yx}, i.e. $\rho_S = \mu_0 R_S M_S$, is determined from the measured isotherms by extrapolation of the linear high-field part of ρ_{yx} to zero internal induction. The value of ρ_S is negative for all temperatures up to 340 K (figure 18 (curve A)). Division by the measured saturation magnetisation (figure 14 (curve A)) gives R_S. The temperature dependence of R_S (figure 19 (curve A)) is as expected for collinear ferromagnets (Berger and Bergmann 1980): the absolute value of R_S increases with increasing temperature up to T_C.

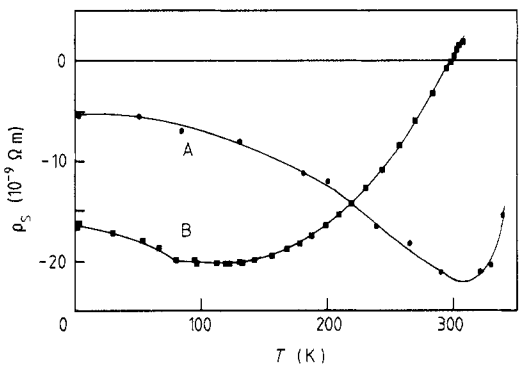

Figure 18. Spontaneous part of the Hall resistivity $\rho_S = \mu_0 R_S M_S$ of hexagonal $Cr_{0.9}Te$ (curve A) and monoclinic $Cr_{0.8}Te$ (curve B).

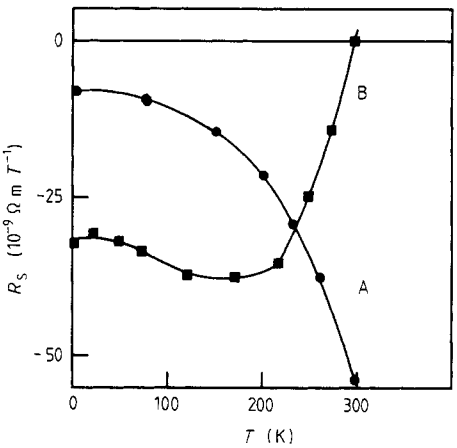

Figure 19. Temperature dependence of the spontaneous Hall coefficient R_S of hexagonal $Cr_{0.9}Te$ (curve A) and monoclinic $Cr_{0.8}Te$ (curve B).

The slope $\partial\rho_{yx}/\partial B_A$ in the high-field region is

$$\partial\rho_{yx}/\partial B_A = R_0 + \chi_i R_S$$

where $B_A = \mu H_A$ and χ_i is the internal magnetic susceptibility above technical saturation. For temperatures well below T_C, χ_i is very small and $\partial\rho_{yx}/\partial B_A$ directly gives $R_0 = +1.5 \times 10^{-9}$ Ω m T^{-1}. This value corresponds to $p = 0.2$ holes per formula unit $Cr_{0.9}Te$, in a single carrier formalism ($p = (eR_0)^{-1}$).

4.4.2. $Cr_{0.8}Te$. The Hall resistivity ρ_{yx} of single-crystalline $Cr_{0.8}Te$, belonging to the monoclinic Cr_3Te_4 phase, was measured in the temperature range from 4.2 to 330 K (figure 20). The magnetic field was applied normal to the *ab* plane. Except for anisotropy, saturation is reached at an applied field of about $N_D M$, with demagnetising factor N_D of 1 for the thin platelet that was used.

However, the temperature dependence of the extrapolated value of the Hall resistivity, the so-called spontaneous Hall resistivity $\rho_S = \mu_0 R_S M$ (figure 18 (curve B)), strongly deviates from the behaviour usually found in collinear ferromagnets: ρ_S has already a large negative value at 4.2 K, it shows a minimum around 100 K and changes sign at 300 K. The minimum in ρ_S occurs at temperature T_s (see figure 14 (curve B)). The temperature dependence of R_S (figure 19 (curve B)) shows the same characteristics as ρ_S.

The usually observed temperature dependence of R_S is an increase of R_S up to T_C and a nearly constant R_S value above T_C. However, R_S or better ρ_S of $Cr_{0.8}Te$ shows a very different behaviour. One possible explanation is that the total ρ_S of $Cr_{0.8}Te$ consists of two contributions with opposite sign. One of these, ρ_{S1}, has a negative sign and a transition temperature of $T_s \simeq 100$ K and is constant above T_s. The other, ρ_{S2}, has a positive sign and a transition temperature T_C. At 0 K, ρ_{S1} must have already a large negative value and below T_s it increases more strongly in absolute magnitude than ρ_{S2} below T_s. Above T_s, ρ_{S1} is constant and the temperature dependence of ρ_{S2} becomes more apparent. An interpretation of the origin of ρ_{S1} and ρ_{S2} is hampered by lack of knowledge of the magnetic structure of Cr_3Te_4 above and below T_s.

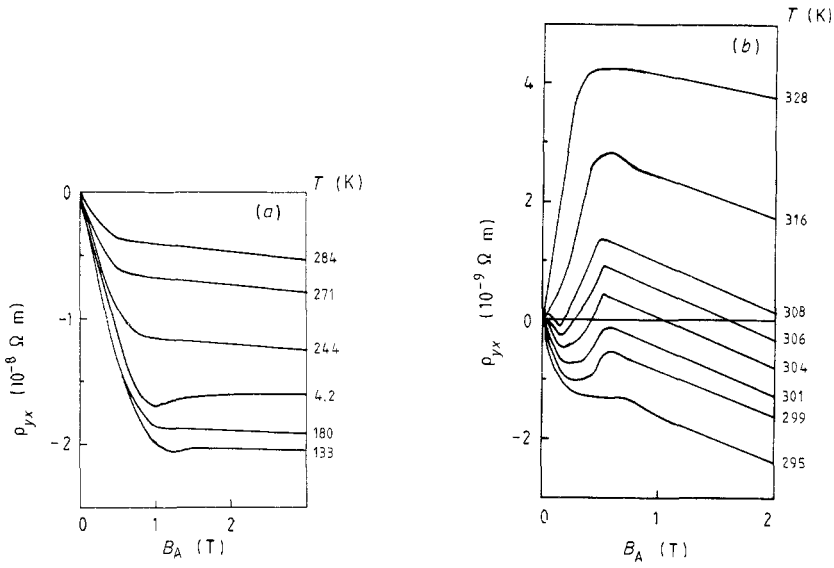

Figure 20. Measured Hall resistivities ρ_{yx} of monoclinic $Cr_{0.8}Te$.

However, it is unlikely that the measured temperature dependence of ρ_S in $Cr_{0.8}Te$ can be explained by a simple collinear ferromagnetic spin structure, which is usually assumed in the temperature range between T_s and T_C.

This conclusion is sustained by the ρ_{yx} measurements near 300 K (figure 20(*b*)), which show anomalous behaviour in the low-field region below 0.5 T. These complicated isotherms were exactly reproducible. The slope at fields above 0.5 T is equal to R_0, which is negative.

A speculative explanation of the field dependence of ρ_{yx} (Weitering 1986) can be given, assuming two magnetic sublattices with different anisotropy constants and ρ_{Si} values of about the same magnitude, but of opposite sign. This intricate behaviour will become apparent only in the temperature range where both contributions to the spontaneous Hall effect nearly compensate each other. The anisotropy of the sublattice with positive ρ_S must have the large anisotropy constant, so that at low fields the negative ρ_S predominates, while at somewhat higher fields the positive ρ_S becomes dominant.

4.5. Discussion

The complex magnetic behaviour, and consequently the complex behaviour of the Hall effect, of chromium tellurides is a consequence of competing exchange interactions of opposite sign (Grazhdankina *et al* 1976a, b). The large residual resistivity measured for $Cr_{0.8}Te$ and $Cr_{0.9}Te$ (figure 15), which is of the same order of magnitude as the spin-disorder resistivity, indicates that there must be a large number of defects at $T = 0$ K. The presence of alternating, completely filled and half-filled Cr layers was proven by x-ray diffraction, but most probably the Cr vacancies are not perfectly ordered within the vacancy layers. It is unknown whether this structural disorder also induces magnetic disorder, but this is not unlikely when competing exchange interactions of opposite sign are present. If an appreciable number of Cr spins have an orientation that deviates from the mean overall alignment, then the net magnetic moment per Cr atom, measured by

neutron diffraction or magnetisation, will be smaller than the local moment on each Cr atom.

5. Concluding remarks

The compound $Cr_{0.9}Te$ is ferromagnetic, with a saturation magnetisation of 2.43 μ_B per formula unit $Cr_{0.9}Te$. Neither with magnetic nor with transport (conductivity, thermo-power or Hall-effect) measurements was a low-temperature magnetic phase transition observed. The transport properties of $Cr_{0.9}Te$ indicated definitely metallic behaviour. The opposite sign of the thermo-power (negative) and the normal Hall coefficient (positive) indicates the presence of both (heavy) electrons and (lighter) holes at the Fermi level. The electrons have predominantly Cr 3d character, while the holes come from the top of the Te 5p band, in agreement with the band-structure calculation of CrTe (§ 3.1). The spontaneous Hall effect of $Cr_{0.9}Te$ shows an increase with increasing temperature, as usually observed in ferromagnetic metals.

In $Cr_{0.8}Te$, belonging to the monoclinic Cr_3Te_4 phase, anomalies are observed around 100 K in the magnetic and (spontaneous) Hall-effect measurements. In this temperature region no anomalies were found in the specific resistivity and the thermo-power. At $T_s \simeq 100$ K the antiferromagnetic reflections in the neutron diffractograms disappear, indicating a change from a canted to a collinear ferromagnetic state. However, the temperature dependence of the spontaneous Hall resistivity ρ_S above T_s cannot be explained with a simple collinear spin structure.

The large residual resistivities in $Cr_{0.8}Te$ and $Cr_{0.9}Te$ indicate an appreciable amount of atomic disorder at 0 K. This atomic disorder will probably also influence the magnetic structure.

Band-structure calculations on collinear ferromagnetic CrTe, Cr_3Te_4 and Cr_2Te_3 give magnetisations of 3.51, 3.32 and 3.03 μ_B per Cr atom. These calculations show magnetic moments, localised on the Cr atoms, which are about identical in magnitude (3.3 μ_B) for all three compounds. Direct metal–metal interactions and Cr–Te covalency determine the magnitude of the moments on Cr. As a consequence of the strong Cr–Te covalency the Te 5p bands become magnetically polarised. The variation in Te polarisation—positive in CrTe, about zero in Cr_3Te_4 and negative in Cr_2Te_3—is the main reason for the variation in the net magnetisation per Cr atom in these compounds. The calculated moments are in agreement with the moments deduced from the high-temperature susceptibilties via the Curie–Weiss law. Saturation magnetisations are considerably lower, around 2.4–2.7 μ_B per Cr.

Acknowledgments

We want to thank Dr J L de Boer and Dr K D Bronsema for the CAD4 measurements. One of us (RAdeG) wants to thank the Stichting Fundamenteel Onderzoek der Materie (FOM) for financial support.

References

Andresen A F 1963 *Acta Chem. Scand* **17** 1335
—— 1970 *Acta Chem. Scand.* **24** 3495

Berger L and Bergmann G 1980 *The Hall Effect and its Applications* ed. C L Chien and C R Westgate (New York: Plenum) p 55
Bertaut E F, Roult G, Aleonard R, Pauthenet R, Chevreton M and Jansen R 1964 *J. Physique* **25** 582
Chevreton M 1964 *Thesis* Lyon
Chevreton M, Bertaut E F and Jellinek F 1963 *Acta Crystallogr.* **16** 431
Coehoorn R and de Groot R A 1985 *J. Phys. F: Met. Phys.* **15** 2135
Coehoorn R, Haas C and de Groot R A 1985 *Phys. Rev.* B **31** 1980
de Groot R A, Mueller F M, van Engen P G and Buschow K H J 1983 *Phys. Rev. Lett.* **50** 2024
de Groot R A, van der Kraan A M and Buschow K H J 1986 *J. Magn. Magn. Mater.* **61** 330
Dijkstra J, van Bruggen C F, Haas C and de Groot R A 1989 *J. Phys.: Condens Matter* **1** 9163–74
Grazhdankina N P and Zaynullina R I 1971 *Sov. Phys.–JETP* **32** 1025
Grazhdankina N P, Zaynullina R I and Bersenev Yu S 1976a *Fiz. Tverd. Tella* **18** 3561
Grazhdankina N P, Zaynullina R I and Burkhanov A M 1976b *Fiz. Met. Metallov.* **41** 970
Hamasaki T, Hashimoto T, Yamaguchi Y and Watanabe H 1975 *Solid State Commun.* **16** 895
Haraldsen H and Neuber A 1935 *Z. Anorg. Chem.* **224** 329
Hashimoto T, Hoya K, Yamaguchi M and Ichitsubo I 1971 *J. Phys. Soc. Japan* **31** 679
Hashimoto T and Yamaguchi M 1969 *J. Phys. Soc. Japan* **27** 1121
Hedin L and Lundquist B I 1971 *J. Phys. C: Solid State Phys.* **4** 2064
Hirone T and Chiba S 1960 *J. Phys. Soc. Japan* **15** 1991
Ipser H, Komarek K I and Klepp K O 1983 *J. Less Common Met.* **92** 265
Katoh K and Motizuki K 1987 *J. Phys. Soc. Japan* **56** 655
Lambert-Andron B, Grazhdankina N P and Vettier C 1979 *J. Physique* **39** L43
Lotgering F K and Gorter E W 1957 *J. Phys. Chem. Solids* **3** 238
Makovetskii G I and Shakhlevich G M 1979 *Kristall Technik* **14** 97
Methfessel M and Kübler J 1982 *J. Phys. C: Solid State Phys.* **12** 141
Miller S C and Love W F 1967 *Tables of Irreducible Representations of Space Groups and Co-representations of Magnetic Space Groups* (Boulder: Pruettpress)
Moriya T 1985 *Spin Fluctuations in Itinerant Electron Magnetism* Springer Series in Solid State Sciences vol. 56 (Berlin: Springer)
Motizuki K, Katoh K and Yanase A 1986 *J. Phys. C: Solid State Phys.* **19** 495
Ohsawa A, Yamaguchi Y, Kazama N, Yamaguchi H and Watanabe H 1972 *J. Phys. Soc. Japan* **33** 1303
Ohta S 1985 *J. Phys. Soc. Japan* **54** 1076
Ohta S, Kurosawa S and Anzai S 1981 *J. Phys. Soc. Japan* **51** 1386
Sandratskii L M, Egorov F R and Berdishev A A 1981 *Phys. Status Solidi* b **103** 511
Schwartz K 1986 *J. Phys. C: Solid State Phys.* **16** L211
Shanditsev V A, Vereshchagin L F, Yaskovlev E N, Grazhdankina N P and Alaeva T I 1973 *Sov. Phys.–Solid State* **15** 146
Starichenko B E 1978 *Deposited Doc. VINITI* **77** 2944
Weitering H H 1986 *Internal Report* Laboratory of Inorganic Chemistry, Groningen
Williams A R, Kübler J and Gelatt C D Jr 1979 *Phys. Rev.* B **19** 6094
Wohlfahrt E P 1978 *J. Magn. Magn. Mater.* **7** 113
Yamaguchi M and Hashimoto T 1972 *J. Phys. Soc. Japan* **32** 635
Yanase A and Siratori K 1984 *J. Phys. Soc. Japan* **53** 312
Zaanen J 1986 *Thesis* Groningen
Zaanen J, Sawatzky G A and Allen J W 1985 *Phys. Rev. Lett.* **55** 418